Editors' Suggestion | Featured in Physics

Smaller Grains Are Not Stronger: Microcrystalline Metals at Ultrahigh Strain Rates

Laura Wu,[1] Yuan Yao,[2] Luyan Li,[2] Qi Tang,[2] and Mostafa Hassani[1,2,*]
[1]Department of Materials Science and Engineering, Cornell University, Ithaca, New York 14853, USA
[2]Sibley School of Mechanical and Aerospace Engineering, Cornell University, Ithaca, New York 14853, USA

(Received 8 May 2025; revised 1 October 2025; accepted 17 November 2025; published 9 January 2026)

The strength of metals and alloys increases as grain size decreases due to grain boundary strengthening. This "smaller is stronger" effect has been observed consistently in the microcrystalline, ultrafine-grained, and even nanocrystalline metals with the exception of extremely small grains on the order of ∼10 nm, where grain boundary strengthening breaks down. Here we report a reversed trend in the microcrystalline regime. When subjected to extremely high strain rates, metals with smaller grain sizes become softer. The grain sizes studied here (1–100 μm) are several orders of magnitude larger than those associated with the breakdown of the grain boundary strengthening. We attribute this softening behavior to the suppression of ballistic dislocation transport, which, consequently, limits dislocation-phonon drag in smaller grains.

DOI: 10.1103/yp9h-sr2m

Introduction—Crystalline solids are typically composed of grains separated by planar interfacial defects known as grain boundaries [1]. The interaction between grain boundaries and dislocations [2], the primary carriers of plasticity, plays a critical role in determining the strength of metals [3,4]. The pioneering work of Hall and Petch demonstrated that the strength of metals is inversely proportional to the square root of the grain size [5,6]. This relationship arises because smaller grains limit the number of dislocations that can pile up against grain boundaries [7,8], reducing the associated stress concentration and requiring higher applied stresses to induce yielding in metals [9].

While deviations from the classic Hall-Petch exponent have been observed [10,11], the general trend of increasing strength with decreasing grain size has remained consistent in metals [12]. An exception only arises in extremely small nanocrystalline grains on the order of ∼10 nm [13–15], where the trend reverses to a "negative" or "inverse" relationship between strength and grain size [14,16,17]. In the nanocrystalline regime, as grain size decreases, the dislocation pile-up mechanism and the cumulative contribution to the stress field breaks down [14,18]. However, stress fields transmitted across neighboring grains remains high enough to relax grain boundaries and triple junction by grain boundary sliding [19–21]. This mechanistic transition from dislocation-controlled plasticity to grain boundary-mediated deformation coincides with the emergence of the inverse Hall-Petch effect [14,16,17]. For face-centered cubic (fcc) Cu, this critical grain size is just below 20 nm [15,22]. Despite this transition in the nanocrystalline regime, numerous studies consistently report higher strength with smaller grain sizes in the microcrystalline regime [4,12,23], reinforcing the widely accepted notion that "smaller is stronger."

Here, we report the opposite under extreme strain rates. That, in the microcrystalline regime, metals with smaller grain sizes become softer under supersonic impact. This finding is counterintuitive because, based on the higher grain boundary strengthening [24,25] and strain rate sensitivity of fcc metals [26,27] with smaller grains, one would expect increased strength. This result was made possible by laser-induced microprojectile impact testing (LIPIT) [28–37], which allowed us to study deformation at strain rates approaching $\sim 10^9$ s^{-1} [38,39]. By leveraging the similar deformation geometry and length scale provided by spherical nanoindentation and microprojectile impact, we demonstrate that while the conventional "smaller-stronger" trend holds at low and moderate strain rates, it breaks down at ultrahigh strain rates. We attribute this breakdown to a shift in the dominant deformation mechanism from thermally activated dislocation glide at lower strain rates to dislocation-phonon interactions at ultrahigh strain rates. Through a combination of theoretical developments and carefully designed spherical nanoindentation and impact experiments, we precisely isolate the contribution of dislocation-phonon interactions to plastic deformation. Notably, we report that this mechanism is suppressed as grain size decreases in the microcrystalline regime. Consequently, metals with smaller grains do not benefit as much from this strengthening mechanism as their larger-grained counterparts. These findings can pave the way for designing metals and alloys for extreme conditions through

*Contact author: hassani@cornell.edu

Published by the American Physical Society under the terms of the Creative Commons Attribution 4.0 International license. Further distribution of this work must maintain attribution to the author(s) and the published article's title, journal citation, and DOI.

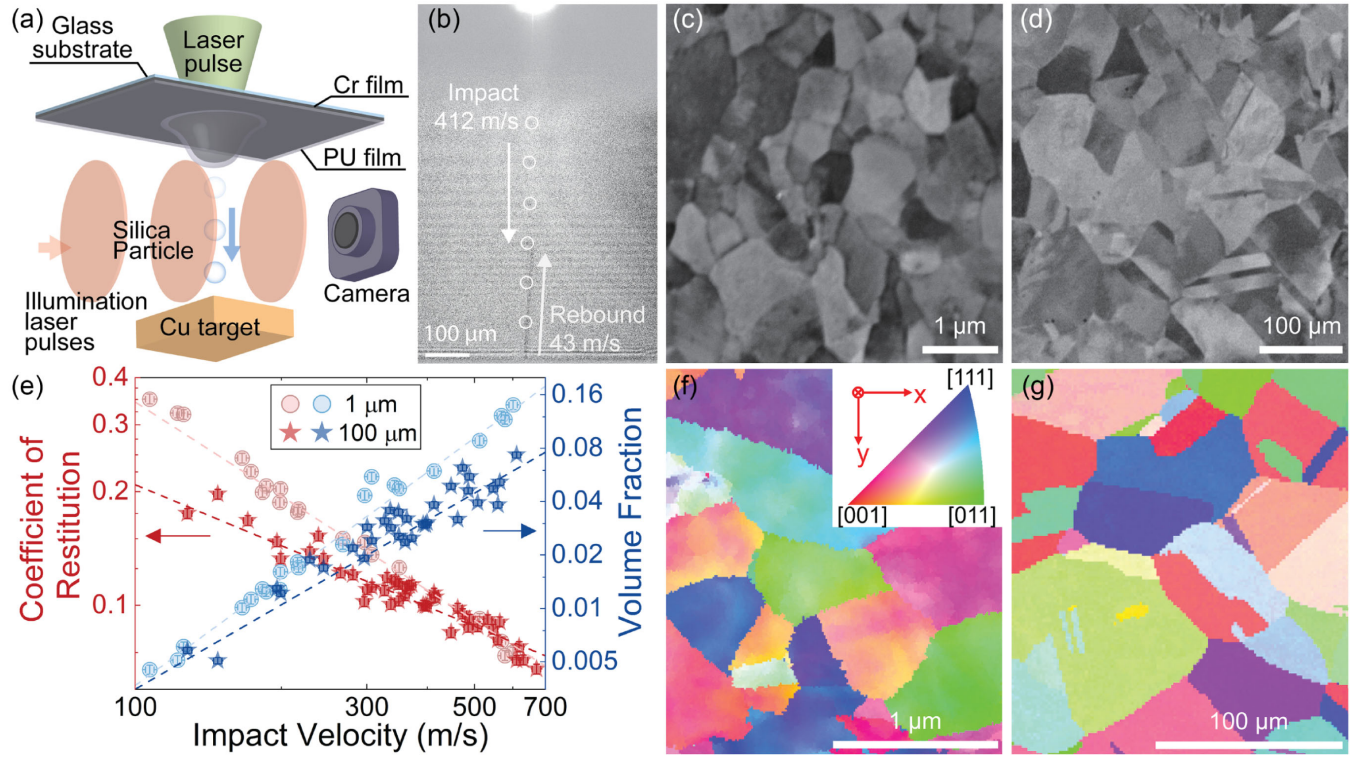


FIG. 1. (a) Schematic of the LIPIT setup. (b) Position of a microprojectile every 398 ns during impact and rebound. SEM images of the Cu microstructure with an average grain size of (c) 1 and (d) 100 μm. (e) Coefficient of restitution and normalized impression volume as a function of impact velocity. EBSD inverse pole figures for Cu with (f) 1 μm and (g) 100 μm grain sizes.

grain boundary engineering to control the dislocation-phonon drag regime.

Results—We used laser-induced microprojectile impact testing (LIPIT) to conduct rigid microprojectile impact experiments on Cu targets [Fig. 1(a) and Supplemental Material Sec. 3 [40]]. The Cu targets have an average grain size of 1 and 100 μm, as shown in the scanning electron microscopy (SEM) images in Figs. 1(c) and 1(d). This grain size range was deliberately selected to remain within the microcrystalline regime where the smaller-stronger trend has consistently been observed. Electron backscatter diffraction (EBSD) analysis confirmed that both microstructures consisted of equiaxed grains [Figs. 1(f) and 1(g)] with negligible orientation gradients within individual grains (Fig. SM1 [40]) and comparable twin fractions (Fig. SM2 [40]). Figure 1(b) shows a representative image from the experiments, resolving the approach, impact, and rebound of a microprojectile. This enables precise measurements of the impact and rebound velocities and thus the kinetic energy dissipated upon impact.

Figure 1(e) shows the coefficient of restitution (COR), defined as the ratio of rebound velocity to impact velocity, as a function of impact velocity for Cu with grain sizes of 1 and 100 μm. At higher impact velocities, a greater fraction of the kinetic energy is dissipated to accommodate increased plastic deformation [38]. As a result, the COR decreases with increasing impact velocity. For a given impact velocity, the 1-μm grain size shows a higher COR compared to the 100-μm grain size, indicating reduced kinetic energy dissipation in smaller grains. This difference is more pronounced at lower impact velocities but diminishes as the impact velocity increases.

For each microprojectile impact, we reconstructed the impact-induced impressions using laser confocal microscopy and measured their volumes. Figure 1(e) shows the normalized impression volume (impression volume divided by microprojectile volume) as a function of impact velocity. As expected, the impression volume increases with higher impact velocities. Interestingly, however, the larger grain size consistently exhibits smaller impression volumes across the entire range of impact velocities studied. Combining these results, we observe that while less plastic work is dissipated during impacts on smaller grain sizes, larger impression volumes are created. These findings suggest that Cu with a 1-μm grain size is softer compared to Cu with a 100-μm grain size.

Using the measured dissipated kinetic energy for each impact and the corresponding impression volume, we can calculate the dynamic hardness of the target material for each impact experiment [31]:

$$H = \frac{W_p}{V} = \frac{E_i \times (1 - \mathrm{COR}^2)}{V}, \tag{1}$$

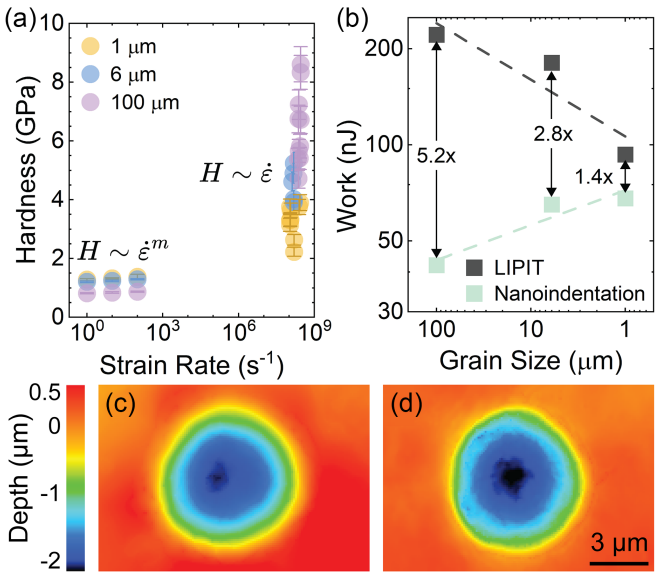


FIG. 2. (a) Hardness measured through nanoindentation and microprojectile impact experiments as a function of strain rate, only including impressions with a fixed nominal strain of 0.21 ± 0.02. (b) Impact and indentation plastic work for impressions with similar volumes as a function of grain size. Laser confocal microscopy reconstructions of microprojectile impact (c) and spherical nanoindentation (d) impressions showing similar volume (48 ± 3 μm^3).

where W_p is the plastic work done during impact, V is the volume of the resulting impression, and E_i is the kinetic energy of the impacting rigid microprojectile. Hardness under quais-static strain rates can be measured from spherical nanoindentation [41], which we combine with the microprojectile impact results in Fig. 2(a), and plot against the effective strain rate across ten decades of strain rates. The effective strain rates in both impact and nanoindentation experiments were calculated using $\dot{\varepsilon} = (v_i/h)$, where v_i is the microprojectile velocity in the impact experiment or the tip velocity in the nanoindentation, and h is the impression depth. To exclude possible strain hardening effects, we have included, in this plot, only data from nanoindentation and impact impression with similar effective strain defined as $\varepsilon = h/(2.4 \times a)$ where a is the half width of the impression [48]. We further analyzed spherical nanoindentation and microprojectile impact data for Cu with a 6 μm grain size from our previous work [38] and included these results in the plot. This enables a direct comparison of the three grain sizes within the microcrystalline regime.

Figure 2(a) clearly reveals two distinct mechanistic regimes. In the low strain rate regime where the thermally activated dislocation glide is the dominant deformation mechanism, the data follows a power-law relationship between hardness and strain rate ($H \propto \dot{\varepsilon}^m$, $m < 1$). In contrast, at ultrahigh strain rates, there is a sharp increase in dynamic hardness, exhibiting a linear trend ($H \propto \dot{\varepsilon}$) that is the characteristic of the dislocation-phonon drag regime [49,50]. As the grain size decreases from 100 to 1 μm, the strain rate sensitivity shows a modest increase from 0.014 to 0.016 in the thermal activation region, consistent with previously reported trends in the thermally activated regime [51–54]. We also observe a clear grain boundary strengthening effect in this regime, following the smaller-stronger trend. These findings are expected and consistent with well-documented Hall-Petch effect [4–6,12] and strain rare sensitivity for FCC metals [53,55] in this regime of deformation.

In the ultrahigh strain rate regime, on the other hand, we observe a reverse trend. Our microprojectile impact experiments reveal that the hardness of Cu decreases as the grain size decreases from 100 to 1 μm. This reversal of the conventional smaller-stronger trend in the microcrystalline regime is unexpected. It suggests a dominant deformation mechanism that overshadows the conventional strengthening from the dislocation-grain boundary interactions. Specifically, the interaction of fast-moving dislocations with phonons, resulting in dislocation drag [39,56], is known to contribute an additional hardening component at high strain rates [37–39]. Our findings suggest that dislocation-phonon drag not only emerges but becomes the primary hardening mechanism under these extreme conditions. More interestingly, our results suggest that the contribution of dislocation-phonon drag to the overall hardening decreases as the grain size becomes smaller, implying that dislocation-phonon drag is suppressed in the smaller grains. We attribute this suppression to reduced ballistic transport of dislocations in finer grains, which lowers the intensity of dislocation-phonon interactions. As a result, the overall hardness of the metal is reduced at ultrahigh strain rates.

We adjusted the impact velocity and nanoindentation depth to achieve similar deformation geometries and volumes, enabling a direct comparison between thermally activated dislocation glide in nanoindentation and dislocation-phonon drag in microprojectile impact. Representative indents with a volume of 48 ± 3 μm^3 were selected for the data presented in Fig. 2(b). The more than fivefold increase in impact plastic work compared to nanoindentation measured for the 100-μm grain size arises from the transition from thermal activation to phonon drag. While the plastic work from nanoindentation increases as the grain size decreases, the plastic work from microprojectile impact exhibits a decreasing trend. Specifically, the ratio between the impact and nanoindentation plastic work narrows from 5.2 times at the 100-μm grain size to 2.8 and 1.4 times at the 6- and 1-μm grain sizes, respectively. This trend again suggests a reduced contribution of dislocation-phonon interactions at ultrahigh strain rates and a corresponding suppression of dislocation-phonon drag as grain sizes decrease.

Theoretical framework to quantify the dislocation-phonon interactions: While the results presented in Fig. 2

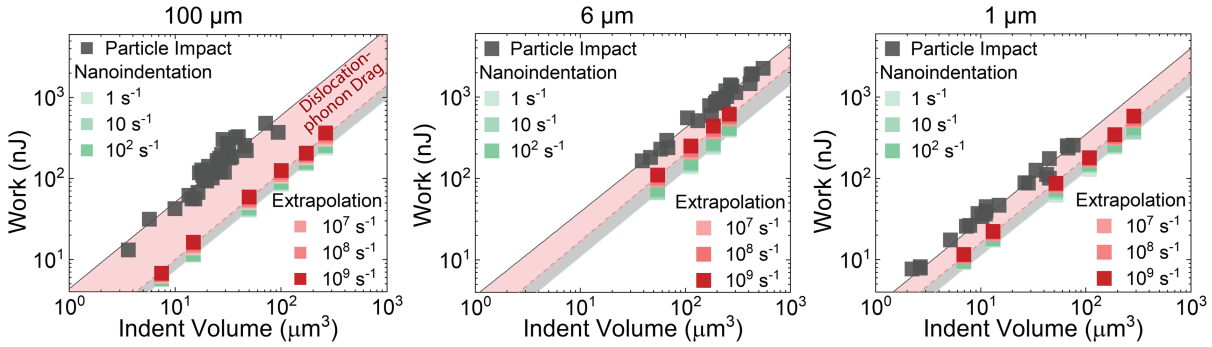


FIG. 3. Plastic work as a function of the impression volume distinguishing the thermal activation and dislocation-phonon drag contributions for Cu with different grain sizes.

suggest a suppression of dislocation-phonon interactions with decreasing grain size, they remain mostly qualitative. The increase in plastic work from nanoindentation to microprojectile impact consists of contributions from both thermal activation and phonon drag [38,39]. To accurately isolate the contribution of dislocation-phonon interactions, we develop a theoretical framework grounded on classical dislocation mechanics. This framework relies on the principle that measurements of plastic work through nanoindentation at varying strain rates exclusively reflect the thermal activation regime and establish a rigorous functional form to extrapolate it to the ultrahigh strain rates associated with microprojectile impacts. We can then subtract the extrapolated thermal activation contribution from the total plastic work measured during microprojectile impact experiments to isolate the dislocation-phonon drag contribution and compare it across different grain sizes. As a starting point, we revisit the classic equation describing the strain rate and temperature dependency of stress within the thermal activation regime, σ_{th} [57]:

$$kT\ln\left(\frac{\dot{\varepsilon}_0}{\dot{\varepsilon}}\right) = g_0\mu b^3\left[1-\left(\frac{\sigma_{\mathrm{th}}}{\sigma_0}\right)^p\right]^q, \tag{2}$$

where σ_0 is the threshold stress required for dislocation glide without thermal energy (i.e., at 0 K). The role of thermal energy is to decrease the stress required for the dislocation to bypass obstacles from σ_0 to σ_{th} at finite temperatures T and at strain rates $\dot{\varepsilon}$, smaller than a reference strain rate $\dot{\varepsilon}_0 = 2\times10^{10}\ \mathrm{s}^{-1}$. The $g_0\mu b^3$ represents obstacles' barrier energy with g_0 being a constant, b being the magnitude of the Burgers vector, and μ being the shear modulus. Exponents p and q are constants related to the shape and spacing of the obstacles.

In the Supplemental Material Sec. 6 [40], we show that the thermal activation equation can be mapped from the stress space [Eq. (2)] into the plastic work space by introducing an indentation plastic work, W_p, and a volume-dependent threshold plastic work for indentation, W_{p0}:

$$(W_p)^p = (W_{p0})^p - \frac{(W_{p0})^p}{g_0^{\frac{1}{q}}}\left[\frac{kT}{\mu b^3}\ln\left(\frac{\dot{\varepsilon}_0}{\dot{\varepsilon}}\right)\right]^{\frac{1}{q}}. \tag{3}$$

Based on Eq. (3), a linear relationship between $(W_p)^p$ and $[(kT/\mu b^3)\ln(\dot{\varepsilon}_0/\dot{\varepsilon})]^{(1/q)}$ is expected in the thermal activation regime. Figure SM3 [40] confirms that this is indeed the case for all three grain sizes. We can use this linear trend to extrapolate the contribution of thermal activation to deformation at ultrahigh strain rates, comparable to those induced by microprojectile impact (10^7–$10^9\ \mathrm{s}^{-1}$). By subtracting this thermally activated component from the measured total plastic work, we isolate the contribution arising from phonon drag.

Figure 3 presents the experimentally measured plastic work from spherical nanoindentation and microprojectile impacts as a function of deformation volume. Between these two measurements lie the extrapolated thermal activation plastic work values for strain rates of 10^7–$10^9\ \mathrm{s}^{-1}$. The gray-highlighted gap between the extrapolated values and the nanoindentation data reflects the additional thermal activation contribution resulting from the substantial increase in deformation rate from nanoindentation to microprojectile impact. More significantly, the red-highlighted gap between the microprojectile impact measurements and the thermal activation extrapolation quantifies the additional plastic work caused by the drag effect of dislocation-phonon interactions at ultrahigh strain rates. The data in Fig. 3 clearly demonstrate that this dislocation drag effect diminishes as grain size decreases. On the logarithmic scale of the plastic work axis, the contribution of dislocation-phonon drag to the overall hardening under microprojectile impact conditions is significantly larger than that of thermally activated processes. As a result, the reduction in dislocation drag at smaller grain sizes leads directly to metal softening under ultrahigh strain rate conditions.

Using the data presented in Fig. 3, we isolate the plastic work arising exclusively from interactions between fast-moving dislocations and phonons ($W_{p,D}$) and plot it as a function of indentation volume in Fig. 4. By rewriting the

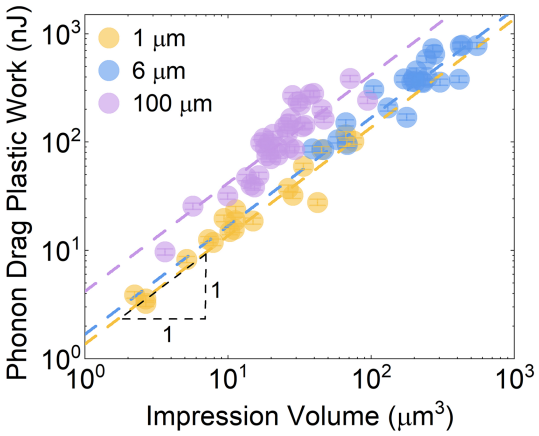


FIG. 4. Phonon drag plastic work as a function of impression volume for Cu with grain size of 1, 6, and 100 μm. The data exhibit a slope of unity, while the intercept defines the effective phonon-drag hardness.

classical definition of dynamic hardness [Eq. (1)] for the drag regime, we define an effective phonon drag hardness, H_D, for each grain size in Eq. (4). This quantity represents an effective resistance to plastic deformation associated with the dislocation-phonon drag regime. The log-log plot of drag plastic work versus impression volume in Fig. 4 exhibits a slope of unity consistent with Eq. (4). The intercepts with the phonon drag plastic work axis show the effective phonon drag hardness. Notably, Cu with a grain size of 100 μm exhibits the highest effective phonon drag hardness of 4.19 GPa, which decreases to 1.37 GPa for Cu with a 1 μm grain size.

$$H_D = \frac{W_{p,D}}{V}. \tag{4}$$

Discussion—To accommodate the ultrahigh strain rates induced by impact, dislocations accelerate to relatively high steady-state velocities, where they begin to interact with phonons [38,39,56]. The intensity of this interaction is directly proportional to the steady-state velocity of dislocations [50], which is influenced by the available mean free path for dislocation acceleration [42] and the resolved shear stress [57] driving the glide process. Both factors are affected by changes in grain size. Grain boundaries and dislocation cell structures within grains act as barriers to dislocation motion, decelerating or halting their glide [5,6]. Larger grains allow for larger substructures (e.g., dislocation cells), increasing the mean free path and enabling dislocations to achieve higher velocities. Conversely, as grain size decreases, dislocations become more confined, reducing the terminal velocity and diminishing the intensity of their interaction with phonons.

Additionally, smaller grain sizes reduce the level of stress available for accelerating dislocations. The stress driving dislocation glide is the portion of the flow stress that remains after accounting for the thresholds for both thermal activation and athermal processes [Eq. (S5) [40]]. While the thermal component is grain size independent, the athermal component is strongly grain size dependent due to grain boundary strengthening. The well-documented Hall-Petch data for Cu [12] shows that as grain size decreases from 100 to 1 μm, the athermal stress component increases by a factor of 3 [Eq. (S6) [40]]. The lower flow stress during microprojectile impact in Cu with 1-μm grain size together with the higher athermal stress reduces the applied shear stress available to accelerate dislocations. Our first-order approximation shows a noticeable drop in the applied shear stress by a factor of 3 when grain size reduces from 100 to 1 μm [39]. As grain size decreases, the combined effects of reduced mean free path and lower applied shear stress result in a slower terminal steady-state velocity of dislocations. This further results in lower levels of dislocation-phonon interactions, decreasing dislocation drag hardening and ultimately leading to a softening behavior under extreme strain rates.

A wide range of grain sizes, such as those studied here, can potentially influence the susceptibility of different microstructures to adiabatic shear banding. In our case, measurements of effective hardness are derived from the coefficient of restitution and the total deformation volume. Any potential shear banding—if it occurs—would likely be confined to localized regions at the periphery of the impressions and should have minimal impact on the measured values. Previous studies on Cu in the microcrystalline regime have reported a higher propensity for adiabatic shear banding at larger grain sizes, attributed to twinning activity [58,59]. When combined with our present observation that larger grains exhibit higher hardness, these results suggest that dislocation-drag hardening likely dominates and outweighs competing mechanisms under the conditions of the present experiments.

Conclusions—In summary, we conducted spherical nanoindentation and microprojectile impact experiments on a model fcc metal, Cu. Our findings reveal that while smaller grain sizes increase strength at lower deformation rates, the trend reverses under ultrahigh strain rates. Under microprojectile impact at a fixed velocity, Cu with smaller grains dissipates less kinetic energy yet exhibits larger impact impressions, indicating a transition to a softer response compared to its large-grained counterparts. We attribute this behavior to a shift in the dominant deformation mechanism—from thermally activated dislocation glide at low strain rates to ballistic dislocation transport and phonon drag at high strain rates. To quantify this effect, we developed a theoretical framework that, combined with our indentation and impact measurements, isolates the contribution of phonon drag to plastic deformation. Our analysis shows that phonon drag is suppressed as grain size decreases. Since phonon drag is the primary strengthening mechanism at extreme strain rates, its suppression directly

leads to a softening of metals with finer grains. Although the findings of this Letter are derived for an FCC structure, the transition from thermally activated dislocation glide to dislocation-phonon interactions is a universal phenomenon. The underlying principles should therefore be broadly applicable to other crystal structures, which we leave as a direction for future studies.

Acknowledgments—We gratefully acknowledge the funding received by the National Science Foundation (CMMI-2406597). This research was also, in part, sponsored by the Army Research Office under Cooperative Agreement No. W911NF-25-2-0048.

Data availability—The data that support the findings of this article are not publicly available upon publication because it is not technically feasible and/or the cost of preparing, depositing, and hosting the data would be prohibitive within the terms of this research project. The data are available from the authors upon reasonable request.

[1] K. Lu, L. Lu, and S. Suresh, Strengthening materials by engineering coherent internal boundaries at the nanoscale, Science **324**, 349 (2009).
[2] H. Fan, Q. Wang, J. A. El-Awady, D. Raabe, and M. Zaiser, Strain rate dependency of dislocation plasticity, Nat. Commun. **12**, 1845 (2021).
[3] L. Lu, Y. Shen, X. Chen, L. Qian, and K. Lu, Ultrahigh strength, and high electrical conductivity in copper, Science **304**, 422 (2004).
[4] N. Hansen and B. Ralph, The strain and grain size dependence of the flow stress of copper, Acta Metall. **30**, 411 (1982).
[5] E. O. Hall, The deformation and ageing of mild steel: III discussion of results, Proc. Phys. Soc. London Sect. B **64**, 747 (1951).
[6] N. J. Petch, The cleavage strength of polycrystals, J. Iron Steel Inst. **174**, 25 (1953).
[7] H. Van Swygenhoven, Grain boundaries and dislocations, Science **296**, 66 (2002).
[8] J. Hu, Y. N. Shi, X. Sauvage, G. Sha, and K. Lu, Grain boundary stability governs hardening, and softening in extremely fine nanograined metals, Science **355**, 1292 (2017).
[9] E. N. Hahn and M. A. Meyers, Grain-size dependent mechanical behavior of nanocrystalline metals, Mater. Sci. Eng. **646**, 101 (2015).
[10] D. J. Dunstan and A. J. Bushby, Grain size dependence of the strength of metals: The Hall–Petch effect does not scale as the inverse square root of grain size, Int. J. Plast. **53**, 56 (2014).
[11] T. Narutani and J. Takamura, Grain-size strengthening in terms of dislocation density measured by resistivity, Acta Metall. Mater. **39**, 2037 (1991).
[12] Z. C. Cordero, B. E. Knight, and C. A. Schuh, Six decades of the Hall–Petch effect—A survey of grain-size strengthening studies on pure metals, Int. Mater. Rev. **61**, 495 (2016).
[13] C. A. Schuh, T. G. Nieh, and T. Yamasaki, Hall–Petch breakdown manifested in abrasive wear resistance of nanocrystalline nickel, Scr. Mater. **46**, 735 (2002).
[14] M. A. Meyers, A. Mishra, and D. J. Benson, Mechanical properties of nanocrystalline materials, Prog. Mater. Sci. **51**, 427 (2006).
[15] T. G. Nieh and J. Wadsworth, Hall-Petch relation in nanocrystalline solids, Scr. Metall. Mater. **25**, 955 (1991).
[16] J. Schioøtz and K. W. Jacobsen, A maximum in the strength of nanocrystalline copper, Science **301**, 1357 (2003).
[17] J. Schiøtz, F. D. Di Tolla, and K. W. Jacobsen, Softening of nanocrystalline metals at very small grain sizes, Nature (London) **391**, 561 (1998).
[18] G. M. Cheng, W. W. Jian, W. Z. Xu, H. Yuan, P. C. Millett, and Y. T. Zhu, Grain size effect on deformation mechanisms of nanocrystalline BCC metals, Mater. Res. Lett. **1**, 26 (2013).
[19] D. Jia, K. T. Ramesh, and E. Ma, Effects of nanocrystalline and ultrafine grain sizes on constitutive behavior and shear bands in iron, Acta Mater. **51**, 3495 (2003).
[20] T. J. Rupert, D. S. Gianola, Y. Gan, and K. J. Hemker, Experimental observations of stress-driven grain boundary migration, Science **326**, 1686 (2009).
[21] G. Palumbo, U. Erb, and K. T. Aust, Triple line disclination effects on the mechanical behaviour of materials, Scr. Metall. Mater. **24**, 2347 (1990).
[22] A. H. Chokshi, A. Rosen, J. Karch, and H. Gleiter, On the validity of the Hall-Petch relationship in nanocrystalline materials, Scr. Metall. **23**, 1679 (1989).
[23] D. A. Curry, Grain-size dependence of cleavage fracture toughness in mild steel, Nature (London) **276**, 50 (1978).
[24] N. Hansen, Hall–Petch relation and boundary strengthening, Scr. Mater. **51**, 801 (2004).
[25] K. Lu, L. Lu, and S. Suresh, Strengthening materials by engineering coherent internal boundaries at the nanoscale, Science **324**, 349 (2009).
[26] R. Schwaiger, B. Moser, M. Dao, N. Chollacoop, and S. Suresh, Some critical experiments on the strain-rate sensitivity of nanocrystalline nickel, Acta Mater. **51**, 5159 (2003).
[27] Q. Wei, Strain rate effects in the ultrafine grain and nanocrystalline regimes-influence on some constitutive responses, J. Mater. Sci. **42**, 1709 (2007).
[28] J. H. Lee, D. Veysset, J. P. Singer, M. Retsch, G. Saini, T. Pezeril, K. A. Nelson, and E. L. Thomas, High strain rate deformation of layered nanocomposites, Nat. Commun. **3**, 1 (2012).
[29] Q. Tang, D. Veysset, H. Assadi, Y. Ichikawa, and M. Hassani, Strength gradient in impact-induced metallic bonding, Nat. Commun. **15**, 1 (2024).
[30] M. Hassani, D. Veysset, Y. Sun, K. A. Nelson, and C. A. Schuh, Microparticle impact-bonding modes for mismatched metals: From co-deformation to splatting and penetration, Acta Mater. **199**, 480 (2020).
[31] M. Hassani, D. Veysset, K. A. Nelson, and C. A. Schuh, Material hardness at strain rates beyond 10^6 s − 1 via high velocity microparticle impact indentation, Scr. Mater. **177**, 198 (2020).

[32] M. Hassani-Gangaraj, D. Veysset, K. A. Nelson, and C. A. Schuh, *In-situ* observations of single micro-particle impact bonding, Scr. Mater. **145**, 9 (2018).
[33] M. Hassani-Gangaraj, D. Veysset, K. A. Nelson, and C. A. Schuh, Melt-driven erosion in microparticle impact, Nat. Commun. **9**, 5077 (2018).
[34] R. Thevamaran, O. Lawal, S. Yazdi, S. J. Jeon, J. H. Lee, and E. L. Thomas, Dynamic creation and evolution of gradient nanostructure in single-crystal metallic microcubes, Science **354**, 312 (2016).
[35] J. H. Lee, P. E. Loya, J. Lou, and E. L. Thomas, Dynamic mechanical behavior of multilayer graphene via supersonic projectile penetration, Science **346**, 1092 (2014).
[36] D. Veysset, J. H. Lee, M. Hassani, S. E. Kooi, E. L. Thomas, and K. A. Nelson, High-velocity micro-projectile impact testing, Appl. Phys. Rev. **8**, 011319 (2021).
[37] I. Dowding and C. A. Schuh, Metals strengthen with increasing temperature at extreme strain rates, Nature (London) **630**, 91 (2024).
[38] Q. Tang and M. Hassani, Quantifying dislocation drag at high strain rates with laser-induced microprojectile impact, Int. J. Plast. **175**, 103924 (2024).
[39] Q. Tang, J. Li, B. C. Hornbuckle, A. Giri, K. Darling, and M. Hassani, Suppressed ballistic transport of dislocations at strain rates up to 10 s in a stable nanocrystalline alloy, Commun. Mater. **6**, 1 (2025).
[40] See Supplemental Material at http://link.aps.org/supplemental/10.1103/yp9h-sr2m for details on methods, extrapolation in our theoretical framework, and applied shear stress calculations, which includes Refs. [5,6,12,41–47].
[41] W. C. Oliver and G. M. Pharr, An improved technique for determining hardness and elastic modulus using load and displacement sensing indentation experiments, J. Mater. Res. **7**, 1564 (1992).
[42] S. A. Turnage, M. Rajagopalan, K. A. Darling, P. Garg, C. Kale, B. G. Bazehhour, I. Adlakha, B. C. Hornbuckle, C. L. Williams, P. Peralta, and K. N. Solanki, Anomalous mechanical behavior of nanocrystalline binary alloys under extreme conditions, Nat. Commun. **9**, 2699 (2018).
[43] Y. S. Li, Y. Zhang, N. R. Tao, and K. Lu, Effect of thermal annealing on mechanical properties of a nanostructured copper prepared by means of dynamic plastic deformation, Scr. Mater. **59**, 475 (2008).
[44] D. P. Field, L. T. Bradford, M. M. Nowell, and T. M. Lillo, The role of annealing twins during recrystallization of Cu, Acta Mater. **55**, 4233 (2007).
[45] S. Taylor, I. Masters, Z. Li, and H. R. Kotadia, Direct observation via *in situ* heated stage EBSD analysis of recrystallization of phosphorous deoxidised copper in unstrained and strained conditions, Met. Mater. Int. **26**, 1030 (2020).
[46] L. Dong, F. Yang, T. Yu, N. Zhang, X. Zhou, Z. Xie, and F. Fang, Contribution of grain boundary to strength and electrical conductivity of annealed copper wires, J. Mater. Res. Technol. **26**, 1459 (2023).
[47] W. Luo, H. Gong, Q. Wang, J. Lu, and M. Yan, Effect of cryogenic impact deformation and subsequent annealing on microstructure and microhardness of pure copper, Mater. Lett. **157**, 315 (2015).
[48] S. Pathak and S. R. Kalidindi, Spherical nanoindentation stress–strain curves, Mater. Sci. Eng. **91**, 1 (2015).
[49] G. Regazzoni, U. F. Kocks, and P. S. Follansbee, Dislocation kinetics at high strain rates, Acta Metall. **35**, 2865 (1987).
[50] A. V. Yanilkin, V. S. Krasnikov, A. Y. Kuksin, and A. E. Mayer, Dynamics and kinetics of dislocations in Al and Al–Cu alloy under dynamic loading, Int. J. Plast. **55**, 94 (2014).
[51] Z. N. Mao, X. H. An, X. Z. Liao, and J. T. Wang, Opposite grain size dependence of strain rate sensitivity of copper at low vs high strain rates, Mater. Sci. Eng. **738**, 430 (2018).
[52] G. T. Gray, T. C. Lowe, C. M. Cady, R. Z. Valiev, and I. V. Aleksandrov, Influence of strain rate & temperature on the mechanical response of ultrafine-grained Cu, Ni, and Al − 4Cu − 0.5Zr, Nanostruct. Mater. **9**, 477 (1997).
[53] J. Chen, L. Lu, and K. Lu, Hardness and strain rate sensitivity of nanocrystalline Cu, Scr. Mater. **54**, 1913 (2006).
[54] J. A. Lee, M. Y. Seok, Y. Zhao, I. C. Choi, D. H. Lee, B. B. Seo, U. Ramamurty, T. Y. Tsui, and J. il Jang, Statistical analysis of the size- and rate-dependence of yield and plastic flow in nanocrystalline copper pillars, Acta Mater. **127**, 332 (2017).
[55] C. D. Gu, J. S. Lian, Q. Jiang, and W. T. Zheng, Experimental and modelling investigations on strain rate sensitivity of an electrodeposited 20 nm grain sized Ni, J. Phys. D **40**, 7440 (2007).
[56] V. I. Alshits, The phonon-dislocation interaction and its role in dislocation dragging and thermal resistivity, Mod. Probl. Condens. Matter Sci. **31**, 625 (1992).
[57] M. A. Meyers, *Dynamic Behavior of Materials* (Wiley, New York, 1994).
[58] Y. Yang, J. Huang, X. Lian, and W. Liu, Effect of grain size on adiabatic shear susceptibility of copper, J. Mater. Eng. Perform. **30**, 2798 (2021).
[59] M. A. Meyers, U. R. Andrade, and A. H. Chokshi, The effect of grain size on the high-strain, high-strain-rate behavior of copper, Metall. Mater. Trans. A **26**, 2881 (1995).